

# Dynamical Deep Generative Latent Modeling of 3D Skeletal Motion

Amirreza Farnoosh · Sarah Ostadabbas

Received: date / Accepted: date

**Abstract** In this paper, we propose a Bayesian switching dynamical model for segmentation of 3D pose data over time that uncovers interpretable patterns in the data and is generative. Our model decomposes highly correlated skeleton data into a set of few spatial basis of switching temporal processes in a low-dimensional latent framework. We parameterize these temporal processes with regard to a switching deep vector autoregressive prior in order to accommodate both multimodal and higher-order nonlinear inter-dependencies. This results in a dynamical deep generative latent model that parses the meaningful intrinsic states in the dynamics of 3D pose data using approximate variational inference, and enables a realistic low-level dynamical generation and segmentation of complex skeleton movements. Our experiments on four biological motion data containing bat flight, salsa dance, walking, and golf datasets substantiate superior performance of our model in comparison with the state-of-the-art methods<sup>1</sup>.

**Keywords** 3D skeletal motion · Bayesian inference · Biologically valid interpretation · Generative models · Latent state modeling · Variational inference.

## 1 Introduction

Analyzing 3D motion capture datasets illustrating dynamical motions of a subject is the key processing step in many applications, including highlighting movement patterns of an athlete to optimize their performance,

A. Farnoosh and S. Ostadabbas  
Augmented Cognition Lab, Electrical and Computer Engineering Department, Northeastern University.

<sup>1</sup> The source code, datasets, and rendered 3D models are provided as supplementary materials.

probing behavior of an endangered animal, and monitoring mobility of a patient in a rehabilitation study, to name a few (Moeslund et al., 2006). In all these applications, body pose data contained in the motion capture sequence describes temporal evolution of specific phenomena or tasks and is switching between potentially limited number of states each representing a specific regime.

The efforts in quantifying complex kinematics of biological mechanisms in a lower dimensional subspace has led to the successful design of bio-inspired robots that can mimic their biological counterparts to a great extent (Birch et al., 2000; Gong et al., 2016; Hoff et al., 2016). Many such works have used the statistical methods such as principal component analysis (PCA) (Jolliffe, 1986), for dimensionality reduction. For instance, Santello et al. (1998) showed that 80% of variance of grasping motion in humans can be described by its first two postural synergies. Riskin et al. (2008) discovered that approximating motion of bat wing with only one third of its principal components accounted for 95% of variance of the articulated skeleton.

Motion data segmentation, on the other hand, has been extensively studied in the context of probabilistic PCA and Gaussian mixture model (GMM) (Barbič et al., 2004), kernelized temporal cut (Gong et al., 2012, 2013), sparse subspace clustering (Elhamifar et al., 2015; Xia et al., 2017; Zhou et al., 2020; Xia et al., 2020), kernel k-means and spectral clustering (Zhou et al., 2012), neighborhood graph (Krüger et al., 2016; Wu et al., 2017; Chen et al., 2018), dynamic time warping (Papoutsakis et al., 2017), and topic modeling (Patrón et al., 2018). However, these models are specifically designed for temporal clustering, and inherently do not model temporal dynamics, therefore are not generative.

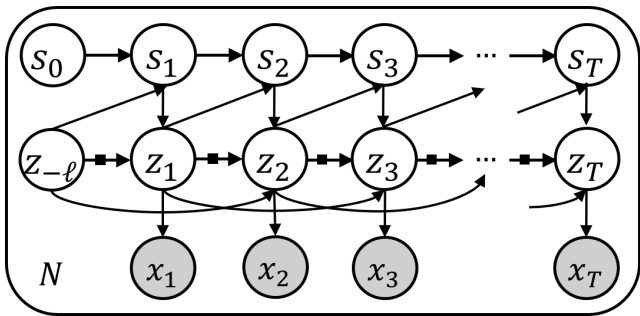


Fig. 1: Graphical representation for our deep switching dynamical model given  $N$  motion datasets. The low-dimensional temporal latents  $Z_n = \{z_{n,t}\}_{t=1}^T$  are generated with regards to a nonlinear vector autoregressive (VAR) prior switched by their associated discrete states  $\mathcal{S}_n = \{s_{n,t}\}_{t=1}^T$ . The discrete states themselves are determined according to a Markovian prior conditioned on their preceding continuous latents, i.e.,  $z_{t-1}$ . The solid black squares represent nonlinear functions. Gray-shaded circles represent observations.

The strong spatio-temporal correlation among joints of a human’s or animal’s skeleton captured by 3D motion capture data as well as clear sparseness in these types of data motivate the utilization of probabilistic models that can learn underlying interpretable states from data and extract its low-dimensional motion patterns. To this end, we propose a Bayesian state switching model for dynamical segmentation of 3D pose data that uncovers interpretable motion patterns and is generative. Specifically, we employ a low-dimensional deep generative latent model to decompose highly correlated skeleton data into a set of few spatial basis of switching auto-regressive temporal processes. This results in a flexible model that accommodates multimodal and higher-order nonlinear inter-dependencies, parses meaningful temporal modes in 3D pose data, and enables low-level dynamical generation and segmentation of complex skeleton movements. We demonstrate superior performance of our model on four biological motion data including bat flight, human salsa dance, walking and golf datasets in terms of learning interpretable states, prediction accuracy, and dynamical generation.

## 2 Related Works

**Dynamical systems modeling** – Switching linear dynamical systems (SLDS) have long been investigated in the literature, [Ackerson and Fu \(1970\)](#); [Chang and Athans \(1978\)](#); [Hamilton \(1990\)](#); [Ghahramani and Hinton \(1996\)](#); [Murphy \(1998\)](#); [Fox et al. \(2009\)](#). These models decompose time series data into series of simpler, repeated dynamical modes represented by discrete and continuous latent states. In SLDS framework, the transitions between discrete states are independent of

their associated continuous values. This problem is addressed in recurrent switching linear dynamical system (rSLDS) ([Linderman et al., 2017](#); [Nassar et al., 2019](#); [Becker-Ehmck et al., 2019](#)), by allowing the discrete state transition probabilities to depend on their preceding continuous states. The rSLDS dynamical capacity is however limited as it assumes first-order linear dynamics. A recent work, ([Farnoosh et al., 2020a](#)), extends these models by adopting nonlinear and higher-order multimodal dependencies through a deep switching autoregressive framework. We build our model on top of this framework and customize that for generative segmentation of motion data. This makes our model flexible for complex auto-regressive relations in motion sequences.

From another perspective, dynamical matrix factorization is used in [Sun et al. \(2014\)](#); [Cai et al. \(2015\)](#); [Bahadori et al. \(2014\)](#); [Yu et al. \(2016\)](#); [Takeuchi et al. \(2017\)](#) for modeling linear dynamics in their low-dimensional temporal factors. Several studies have also employed neural networks for non-linear state-space modeling ([Watter et al., 2015](#); [Karl et al., 2017](#); [Krishnan et al., 2017](#); [Fraccaro et al., 2017](#); [Becker et al., 2019](#); [Farnoosh et al., 2020b](#)), which are restricted to first-order Markovian dependencies, and for time series prediction, ([Chang et al., 2018](#); [Lai et al., 2018](#); [Rangapuram et al., 2018](#); [Li et al., 2019](#); [Sen et al., 2019](#); [Salinas et al., 2020](#)), which most of them are non-probabilistic.

**Motion segmentation** – Segmentation of 3D motion capture data has been studied for many years. Here, we review recent works in this field. [Krüger et al. \(2016\)](#) introduced an automated method for temporal segmentation of human motion data into distinct actions based on a self-similarity matrix extracted from motion sequences of subsequent data points over a window. [Papoutsakis et al. \(2017\)](#) used dynamic time warping (DTW) for co-segmenting all pairs of motion subsequences that represent the same action in an unsupervised manner. [Wu et al. \(2017\)](#) used a combination of normalized cut model and weighted kernel k-means (NCWKK) for behavior segmentation of human motion capture data in its high-dimensional space. [Xia et al. \(2017\)](#) used a sparse subspace clustering framework with geodesic exponential kernel and multi-view reconstruction for motion data segmentation that is able to model their underlying Riemannian manifold and is robust to non-Gaussian noise. [Chen et al. \(2018\)](#) developed a data structure called segment-graph by leveraging information bottleneck method with minimum description length principle to temporally cluster data values via an average-longest-path optimization on this segment-graph. [Patrona et al. \(2018\)](#) per-

formed online action detection and recognition based on an efficient linear search (ELS) approach proposed in Meshry et al. (2016). For this, local features, called gesturelets, capturing both skeleton and kinematics information, are extracted from 3D skeleton joint positions and are subsequently clustered into a bag-of-gesturelets (BoG) model. Then, binary linear classifiers are trained to identify decision boundaries for each specific action. Zhou et al. (2020) proposed a multi level transfer subspace learning framework for human motion segmentation. To capture multi-level structural information, their model factorize labeled source data, from some related task, and target task data into multi-layer feature spaces based on a deep non-negative matrix factorization (NMF) model. Finally, an affinity matrix is constructed and segmentation results are obtained by using the normalized cuts algorithm. Xia et al. (2020) proposed an unsupervised low-rank sparse subspace learning framework with non-convex relaxation for keyframe extraction and segmentation of motion capture data.

Although the aforementioned works are able to cluster motion sequences, they do not explicitly model temporal dynamics, and are not generative. An exception is the work of Nakamura et al. (2017) which proposed a Gaussian process-hidden semi-Markov model (GPHSMM) for unsupervised motion segmentation. However, linear dynamical assumptions in this model fall short of capturing complex temporal dependencies in motion data.

**Our Contributions** – In contrast to previous works which merely cluster motion sequences and are not generative, our method, sketched in Fig. 1, (i) segments motion data from a dynamical perspective by explicitly modeling temporal dynamics, hence, (ii) allows dynamical generation of skeletal movements from low-level representations. Specifically, (iii) it welcomes multimodal, higher-order, and nonlinear temporal relations in motion data by employing a deep switching autoregressive latent model. We focus on four biological motion data including bat flight, human salsa dance, walking, and golf datasets, the first being important in bio-inspired robotic design and the others in activity training as well as human behavior understanding.

### 3 Problem Formulation

We consider a set of  $N$  motion datasets  $\{X_1, \dots, X_N\}$ , where each  $X_n \in \mathbb{R}^{T \times D}$  contains  $T$  time points and  $D$  spatial coordinates (e.g.,  $D = J \times 3$  holds stacked 3D coordinates of  $J$  joints in a human/animal skeleton). We assume that each dataset is generated according to a set of *discrete* latent states  $\mathcal{S}_n = \{s_{n,t}\}_{t=1}^T$  and their

corresponding low-dimensional *continuous* temporal latent variables  $Z_n = \{z_{n,t} \in \mathbb{R}^K\}_{t=1}^T$ :

$$\begin{aligned} X_n &\sim \text{Norm}(L_\theta[Z_n], \sigma^X I), \\ Z_n &\sim p_\theta(Z_n | \mathcal{S}_n), \\ \mathcal{S}_n &\sim p_\theta(\mathcal{S}), \end{aligned} \quad (1)$$

where,  $L_\theta[Z_n]$  is a linear operator that projects local continuous latents  $Z_n$  into the observation space (i.e.,  $L_\theta[Z_n] = Z_n^\top W_\theta$ , where  $W_\theta$  is a projection matrix),  $\sigma^X$  denotes observation noise,  $p_\theta(Z_n | \mathcal{S}_n)$  is a deep switching vector autoregressive (VAR) prior over  $Z_n$  which is parameterized by neural networks, and  $p_\theta(\mathcal{S})$  is a generative Markovian prior over local discrete latents  $\mathcal{S}_n$ . We collectively denote generative model parameters by  $\theta$ . The graphical representation for our proposed generative model is depicted in Fig. 1.

#### 3.1 Discrete Markovian Prior $p_\theta(\mathcal{S})$

We assume that for each dataset the temporal generative process resides at a specific state  $s_t$  at time  $t$  (out of  $S$  possible states) which is determined according to a Markovian prior conditioned on its preceding continuous latent  $z_{t-1}$ . As such, the discrete latent states  $\mathcal{S}_n = \{s_{n,t}\}_{t=1}^T$  are structured in a Markov chain as follows:

$$p_\theta(s_t | s_{t-1} = s, z_{t-1}) = \text{Cat}(\sigma(\Phi_\theta^s z_{t-1})), \quad (2)$$

where  $\Phi_\theta^s \in \mathbb{R}^{S \times K}$  is a state-specific transition matrix and  $\sigma(\cdot)$  is a **softmax** function that ensures a valid  $S$ -dimensional probability vector. As noted in Linderman et al. (2017), conditioning the discrete states on their preceding continuous latents (in addition to their preceding discrete states) is desirable as it allows informed transitions.

#### 3.2 Deep Switching VAR Prior $p_\theta(Z_n | \mathcal{S}_n)$

We assume that the low-dimensional dynamical latents  $Z_n$  follow a nonlinear vector autoregressive Gaussian prior switched by their associated discrete states  $\mathcal{S}_n$ . This implies a Gaussian mixture distribution for the dynamical latent space:

$$p_\theta(z_t | z_{t-\ell}, s_t = s) = \text{Norm}(\mu_\theta^s(z_{t-\ell}), \sigma_\theta^s(z_{t-\ell})), \quad (3)$$

where  $s \in \{1, \dots, S\}$  and  $\ell$  denotes a lag set (e.g.,  $\ell = \{1, 2\}$  for a second-order Markov model), and state-specific  $\mu_\theta^s(\cdot)$  and  $\sigma_\theta^s(\cdot)$  are parameterized by multilayer perceptrons (MLPs) (see Table 1). In other words, we

feed  $z_{t-\ell}$  to a multi-head MLP for estimation of the Gaussian parameters, e.g.,

$$\mu_{\theta}^s(z_{t-\ell}) = \sum_{l \in \ell} \text{MLP}_{\theta}^{s,l}(z_{t-\ell}). \quad (4)$$

### 3.3 Approximate Variational Inference

As the posterior probability for this model is intractable, we use approximate variational methods to learn the model parameters (Hoffman et al., 2013; Ranganath et al., 2013). These methods approximate the posterior of latents  $p_{\theta}(\mathcal{S}, Z | X)$  with a variational distribution  $q_{\phi}(\mathcal{S}, Z)$  by maximizing the evidence lower bound (ELBO):

$$\begin{aligned} \mathcal{L}(\theta, \phi) &= \mathbb{E}_{q_{\phi}(\mathcal{S}, Z)} \left[ \log \frac{p_{\theta}(X, \mathcal{S}, Z)}{q_{\phi}(\mathcal{S}, Z)} \right] \\ &= \log p_{\theta}(X) - \text{KL}(q_{\phi}(\mathcal{S}, Z) \| p_{\theta}(\mathcal{S}, Z | X)) \end{aligned} \quad (5)$$

By maximizing ELBO with respect to the parameters  $\theta$ , we learn a generative model that defines a distribution over datasets  $p_{\theta}(X)$ . By maximizing ELBO over the parameters  $\phi$ , we perform Bayesian inference.

#### 3.3.1 Variational Distribution

We assume a fully factorized variational distribution for the latents  $\{\mathcal{S}, Z\}$ :

$$q_{\phi}(\mathcal{S}, Z) = \prod_{n=1}^N \prod_{t=1}^T q_{\phi}(s_{n,t}) q_{\phi}(z_{n,t}), \quad (6)$$

where  $q_{\phi}(z_{n,t}) = \text{Norm}(\mu_{\phi}^{n,t}, \sigma_{\phi}^{n,t})$ , and the categorical distributions  $q_{\phi}(s_{n,t})$  are approximated with posteriors  $p(s_{n,t} | z_{n,t})$ , where  $z_{n,t} \sim q_{\phi}(z_{n,t})$ , to compensate information loss induced by the mean-field approximation:

$$\begin{aligned} q_{\phi}(s_{n,t} = s) &\simeq p(s_{n,t} = s | z_{n,t}) \\ &= \frac{p_{\theta}(s_{n,t} = s) p_{\theta}(z_{n,t} | s_{n,t} = s)}{\sum_{s=1}^S p_{\theta}(s_{n,t} = s) p_{\theta}(z_{n,t} | s_{n,t} = s)} \end{aligned} \quad (7)$$

#### 3.3.2 ELBO Derivation

We can derive ELBO by plugging in the generative  $p_{\theta}(X, \mathcal{S}, Z)$  and variational  $q_{\phi}(\mathcal{S}, Z)$  distributions from Eq. (1) and Eq. (6) respectively into Eq. (5) (subscript and summation over  $n$  are dropped for brevity):

$$\begin{aligned} -\mathcal{L}(\theta, \phi) &= \\ &\mathbb{E}_{q_{\phi}(Z)} \left[ \|X - L_{\theta}[Z]\|_{\text{F}}^2 \right] + \\ &\sum_t \mathbb{E}_{q_{\phi}(s_{t-1}, z_{t-1})} \left[ \text{KL}(q_{\phi}(s_t) \| p_{\theta}(s_t | s_{t-1}, z_{t-1})) \right] + \\ &\sum_t \mathbb{E}_{q_{\phi}(s_t, z_{t-\ell})} \left[ \text{KL}(q_{\phi}(z_t) \| p_{\theta}(z_t | z_{t-\ell}, s_t)) \right], \end{aligned}$$

Table 1: Network architecture for MLPs parameterizing the Gaussian distribution  $p_{\theta}(z_t | z_{t-\ell}, s_t = s)$ . We defined a fully connected (FC) layer for each state  $s \in \{1, \dots, S\}$ , and lag  $l \in \ell$  as  $\text{FC}_{\theta}^{s,l}$ , the output of which are summed in the succeeding layer according to Eq. (4).

$p_{\theta}(z_t   z_{t-\ell}, s_t = s)$
<b>Input:</b> $z_{t-\ell} \in \mathbb{R}^{ \ell  \times K}$
$[\text{FC}_{\theta}^{s,l} \ K \times K]_{l=1}^{ \ell } \ (\text{PReLU}) \rightarrow (*)$ $\sum_l (*) \rightarrow \text{FC}_{\theta}^s \ K \times K$ <b>Output:</b> $\mu_{\theta}^s \in \mathbb{R}^K$ $(\text{PReLU}) \ \text{FC}_{\theta}^s \ K \times K$ <b>Output:</b> $\log \Sigma_{\theta}^s \in \mathbb{R}^K$

where the three terms correspond to reconstruction loss, discrete latent loss, and continuous latent loss, respectively.

## 4 Implementation Details

We implemented our model in PyTorch v1.3 (Paszke et al., 2017) and run our experiments on an Intel Core i7 CPU@3.7GHz with 8 GB RAM. Our model has  $O(\text{NKT})$  variational and  $O(S|\ell|K^2)$  temporal generative parameters. We employed Adam optimizer (Kingma and Ba, 2014) with  $\text{lr}=\mathbf{0.01}$  and estimated the gradients of ELBO using reparameterization trick, (Kingma and Welling, 2014), for the continuous latent  $Z$ . The expectations over discrete latent  $\mathcal{S}$  are easily handled by summing over all possible states. We trained our model for 1000 epochs and each epoch took from 30 to 500 milliseconds in different experiments.

## 5 Performance Measure

In order to quantify the performance of our dynamical generative model, we compute its temporal predictive error on a test set. To this end, we predict the next time point on a test set using the generative model learned on our train set:  $\hat{x}_{t+1} = L_{\theta}(\hat{z}_{t+1})$ , where  $\hat{z}_{t+1} \sim p(\hat{z}_{t+1} | z_{t+1-\ell}, \hat{s}_{t+1})$  and  $\hat{s}_{t+1} \sim p(\hat{s}_{t+1} | s_t, z_t)$ . We then run inference on  $x_{t+1}$ , the actual observation at  $t+1$ , to obtain  $z_{t+1}$  and  $s_{t+1}$ , and add them to the historical data for prediction of the next time point  $\hat{x}_{t+2}$  in the same way. We repeat these steps to make predictions in a rolling manner across a test set and report their normalized root-mean-square error (NRMSE%). We keep the generative model fixed during the entire prediction. Note that the test set prediction NRMSE% is related to the expected *negative test-set log-likelihood* for our case of Gaussian distributions (with a multiplicative/additive constant).

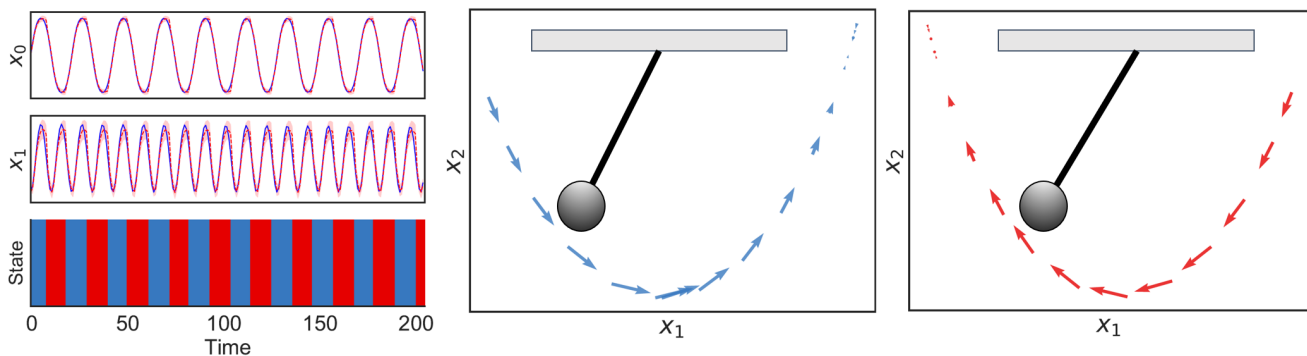


Fig. 2: Inferred states (left) and dynamical trajectories (right) in a pendulum system. The motion in a pendulum system is governed by a second-order nonlinear differential equation. Our model decomposed this motion data into two states: clockwise and anticlockwise rotation. The dynamical trajectory of these two states are visualized using our learned generative model. Our model with lag set  $\ell = \{1, 2\}$  predicted the test set with NRMSE of 5.97% significantly outperforming the baselines. This is expected as the first-order and/or linear transitions in the baselines are not able to effectively model the higher-order and nonlinear dependencies in this system. The true (blue) and predicted (red) 2D coordinates (left-top) are also shown. Red-shaded regions show prediction uncertainty.

## 6 Experimental Results

We evaluated the performance of our proposed generative model in dynamical modeling and segmentation of motion data on a simulated physical system (pendulum system), three human motion data (Salsa dancing, walking and golf) and an animal motion data (bat flight). The generative and predictive performance of our model are summarized in Fig. 2, Fig. 4, Fig. 6, and Table 2.

**Comparison Baselines** – We assessed our model against two established Bayesian switching dynamical models, recurrent switching linear dynamical systems (rSLDS) (Nassar et al., 2019) and switching linear dynamical systems (SLDS) (Fox et al., 2009), a state-of-the-art dynamical matrix factorization method, Bayesian temporal matrix factorization (BTMF) (Sun and Chen, 2019), which models higher-order linear dependencies, a state-of-the-art deep state-space model, recurrent Kalman networks (RKN) (Becker et al., 2019), which employs first-order nonlinear transitions, and a deep neural network forecasting method, long- and short-term time-series network (LSTNet) (Lai et al., 2018), which employs vector auto-regression, throughout the experiments.

### 6.1 Single Pendulum System

A simple pendulum system shares appealing similarities with a joint-angle representation, and its motion is governed by a second-order nonlinear differential equation which makes it an interesting experiment for the purpose of this paper:

$$\ddot{\theta} + g \sin(\theta) = 0 \quad (8)$$

where  $\theta$  is the deflection angle of the pendulum and  $g$  is the gravitational acceleration. We simulated this pendulum system for  $T = 400$  time points and recorded its 2D coordinates. We trained our model (and the baselines accordingly) with lag set  $\ell = \{1, 2\}$ , two states  $S = 2$  and latent dimension  $K = 2$  on half of this dataset and kept the second half for test. Our model decomposed this motion data into two states: clockwise and anticlockwise rotation as depicted in Fig. 3. We have also visualized the dynamical trajectory of these two states using our generative model. Our model predicted the test set with NRMSE of 5.97% (surpassing all the baselines) while rSLDS predicted with 25.58% error. This is expected as the first-order linear transitions in rSLDS are not able to effectively model the higher-order and nonlinear dependencies in this model. Fitting our model with a single lag  $\ell = \{1\}$  increased the error to 7.54%. This is also anticipated as the pendulum equation contains second derivative of location (i.e., acceleration). As reported in Table 2, the linear baselines (rSLDS, SLDS and BTMF) fail to capture the nonlinear transitions and as a result their predictive performance degrades significantly, whereas nonlinear models (Ours, RKN, LSTNet) perform better.

### 6.2 Salsa Dance Dataset

This dataset from CMU MoCap<sup>2</sup> contains 3D coordinates of 19 joints recorded for  $T = 200-571$  time points (every 100 milliseconds) for 15 trials of Salsa dancing. We kept one trial for test, and only used the woman dancer data. We organized this dataset into a tensor of

<sup>2</sup> <http://mocap.cs.cmu.edu/>

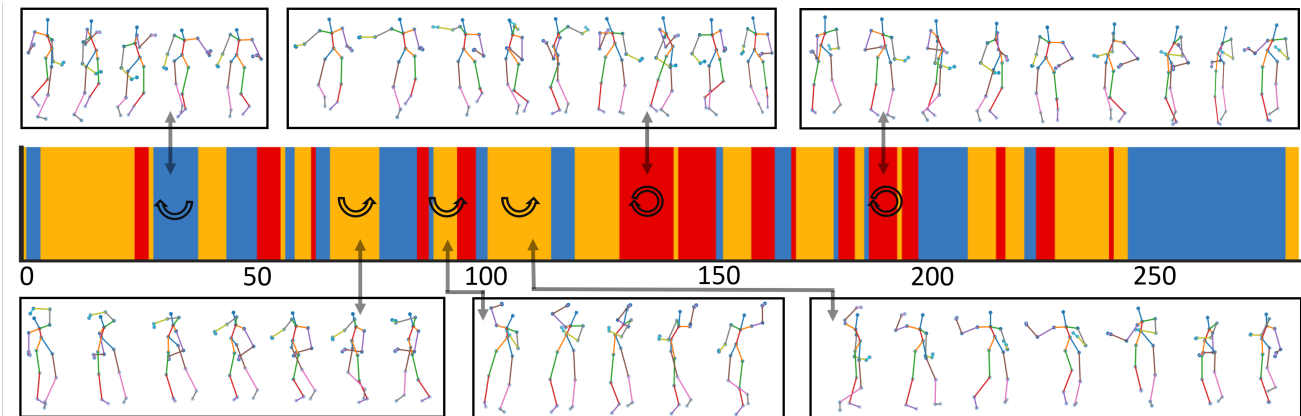


Fig. 3: Inferred states in the test set of salsa dance data. Our model segmented the data into three modes of motion which can be interpreted as: clockwise (CW) turn, anticlockwise (ACW) turn, and twirling motion.

size  $15 \times T \times (19 \times 3)$ . We fit our model (and the baselines accordingly) on this human motion data with  $S = 3$ ,  $\ell = \{1, 2\}$ , and  $K = 10$ . As depicted in Fig. 3, our model segmented the sequences into 3 modes of motion which can be interpreted as: clockwise (CW) turn, anticlockwise (ACW) turn, and twirling motion. We have also computed the dynamical trajectory of each state purely from our learned generative model, and visualized that in Fig. 4. To this end, we just feed the first two time points of the test set to our generative model (since we are using two lags), fix the state, and predict the next 100 time points sequentially using our dynamical generative model (separately for  $s = \{1, 2, 3\}$ ):

$$\begin{aligned} \hat{z}_{t+1} &\sim p_{\theta}(\hat{z}_{t+1} | \hat{z}_{t+1-\ell}, s_{t+1} = s) \\ \hat{x}_{t+1} &= L_{\theta}(\hat{z}_{t+1}) \quad \text{for } t = \{1, \dots, 100\} \end{aligned}$$

This gives us the state-specific dynamical trajectories visualized in Fig. 4 which perfectly follow our interpretation of each state. As reported in Table 2, our model predicted the test set with NRMSE of 6.74% outperforming all the baselines. We have visualized test set predictions along with their uncertainty intervals for two sample joints in Fig. 9 (a). We have rendered the test set and the generated dynamical trajectories for each state on a rigged 3D model of a salsa dancer in **Blender software**, ([Blender Online Community, 2020](#)), and included their videos in our supplementary submission.

### 6.3 Bat Flight Dataset ([Bergou et al., 2015](#))

This dataset includes 3D coordinates of 34 joints on a bat body recorded over time for  $T = 166 - 436$  time points (every 33 milliseconds) during a landing/falling maneuver for 10 experimental runs with 32.55% missing

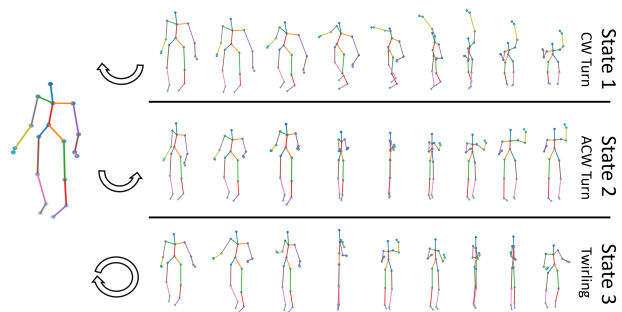


Fig. 4: Dynamical trajectories for each state in the salsa dance data (clockwise (CW) turn, anticlockwise (ACW) turn, and twirling motion). We computed the dynamical trajectory of each state purely from the learned generative model. To this end, we just feed the first two frames of the test set to our generative model, fix the state, and predict the next 100 time points sequentially using our dynamical generative model:  $\hat{z}_{t+1} \sim p_{\theta}(\hat{z}_{t+1} | \hat{z}_{t+1-\ell}, s_{t+1} = s)$  and  $\hat{x}_{t+1} = L_{\theta}(\hat{z}_{t+1})$  for  $t = \{1, \dots, 100\}$ . The predicted dynamical trajectories perfectly follow our interpretation of each state.

values as joint markers are frequently occluded during the flight. We held two runs out for test. We learned our model (and the baselines accordingly) on this data with  $S = 2$ ,  $\ell = \{1, 2\}$ , and  $K = 5$ . As depicted in Fig. 5, our model appears to have parsed the bat flight motion into two modes of “extending” (i.e., stretching the wings), and “flexing” (folding the wings) which together constitute the “flapping” flight in birds. Similar to the Salsa dancing data, we predicted the dynamical trajectory of each state sequentially for 100 time points (entirely from our learned dynamical model), and visualized that in Fig. 6. From this figure, the dynamical trajectory of each state completely support our interpretation of the states. As reported in Table 2, our model predicted the test set with NRMSE of 7.69% outperforming all the baselines. We have also visualized test set predictions

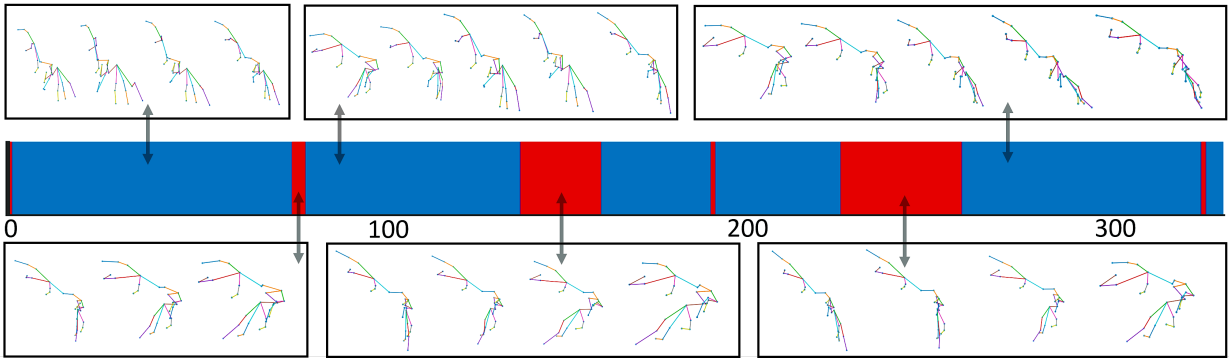


Fig. 5: Inferred states in the test set of bat flight data. Our model has parsed the bat motion into two modes of “extending” and “flexing” which together constitutes the “flapping” flight in birds.

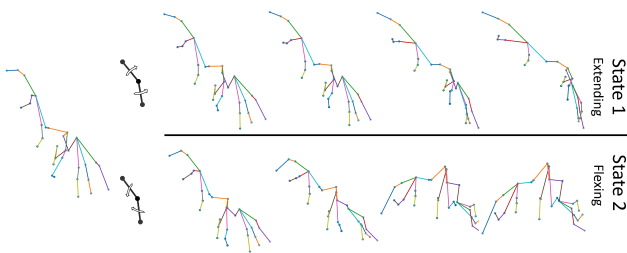


Fig. 6: Dynamical trajectories for each state in bat flight data. We predicted the dynamical trajectory of each state sequentially for 100 time points entirely from our learned dynamical generative model (given the initial frame(s) of the test set). The state-specific dynamical trajectories completely support our interpretation of the states.

along with their uncertainty intervals for two sample joints in Fig. 9 (b). Note that our model fills in missing values for this dataset. We have rendered the test set and the generated dynamical trajectories for each state on a rigged 3D model of a bat in **Blender software**, and included their videos in our supplementary submission.

#### 6.4 Walking Dataset

This is another dataset from CMU MoCap which contains 3D motion capture recordings from a subject for

34 trials of walking/running. We kept two trials for test and trained our model on the rest with  $S = 2$ ,  $\ell = \{1, 2\}$ , and  $K = 5$ . The dynamical segmentation results for the two trials in the test set are visualized in Fig. 7, and show that our model has parsed these locomotion sequences into two phases of “right-leg swing” and “left-leg swing” (encoded by blue and red colors, respectively), which are the familiar components during a bipedal gait cycle. As reported in Table 2, our model predicted the test set with NRMSE of 8.01%, significantly outperforming all of the baselines. We have visualized test set predictions along with their uncertainty intervals for two sample joints in Fig. 9 (d).

#### 6.5 Golf Dataset

This dataset is from the “physical activities and sports” part of CMU MoCap and includes 30 trials of motion recordings from a subject while performing typical actions in a golf game including swing, placing ball, and picking up ball. We kept four trials for test, including two trials of swing and two trials of placing/picking up ball, and trained our model on the rest with  $S = 4$ ,  $\ell = \{1, 2\}$ , and  $K = 10$ . The dynamical segmentation results for the four trials in the test set are visualized in Fig. 8. For swing trials, as pictured in the left side

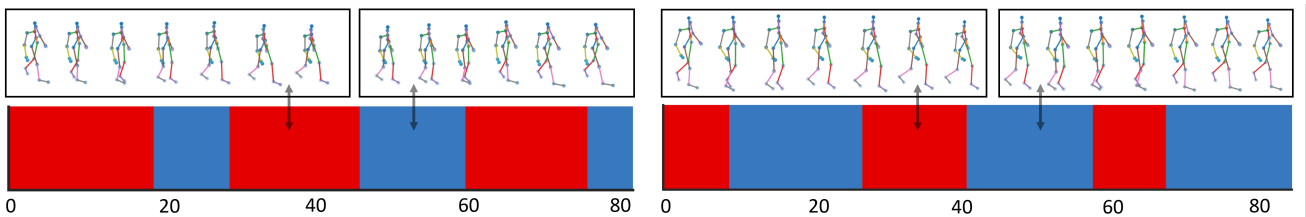


Fig. 7: Inferred dynamical states for the two trials in the test set of walking dataset. Our model has parsed these locomotion sequences into two phases of “right-leg swing”, encoded by the blue color, and “left-leg swing” encoded by the red color, which are the familiar components during a bipedal gait cycle.

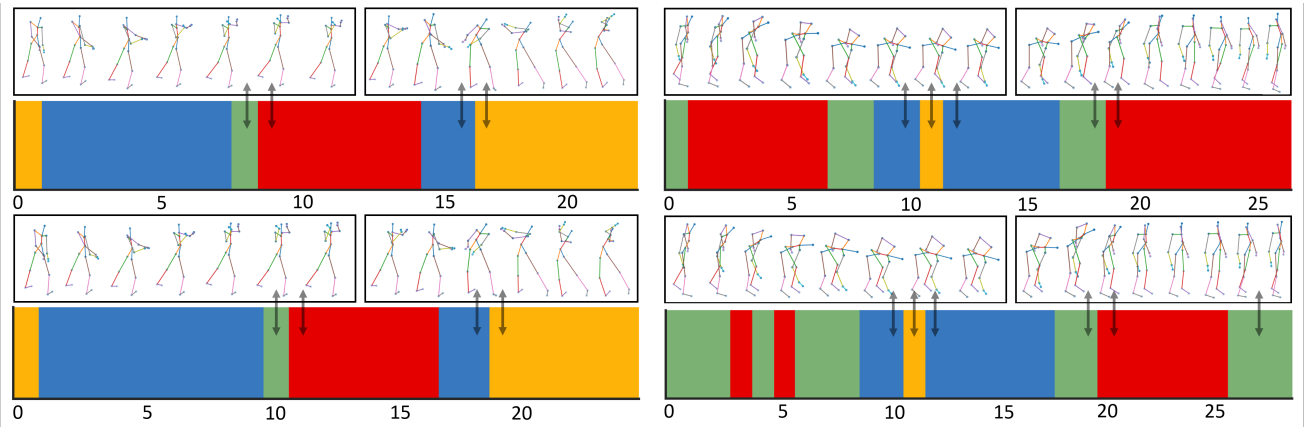


Fig. 8: Inferred dynamical segmentation for the four trials in the test set of golf dataset, including two trials of swing (left) and two trials of placing/picking up ball (right). **Left:** For swing trials, our model divided the swinging motion into major phases of “backswing” (heave+tip point), encoded by the green+red colors, and “downswing” (fall+release), encoded by the blue+yellow colors. **Right:** For the ball placement/pick-up trials, our model split body motion into distinct phases of “bending down”, encoded by the blue+yellow colors, and “standing up”, encoded by the green+red colors.

of Fig. 8, our model divided swinging motion into major phases of “backswing” (heave+tip point), encoded by green+red colors, and “downswing” (fall+release), encoded by blue+yellow colors. Similarly, for the ball placement/pick-up trials in the right side of Fig. 8, our model split body motion into distinct phases of “bending down”, encoded by blue+yellow colors, and “standing up”, encoded by green+red colors. As reported in Table 2, our model predicted the test set with NRMSE of 10.57%, surpassing rSLDS, SLDS, RKN, and LSTNet while closely following BTMF. We have visualized test set predictions along with their uncertainty intervals for two sample joints in Fig. 9 (c).

## 7 Ablation Study

We conducted an ablation study to evaluate the impact of switching feature,  $\mathcal{S}$ , and temporal lags,  $\ell$ , in our model in terms of prediction accuracy. To this end, we executed a version of our model without the switching feature, denoted by **Ours w/o switch**, and a ver-

Table 2: Comparison of prediction error (NRMSE%) on the test sets of pendulum, salsa dance, bat flight, walking and golf datasets. Our model outperforms the baselines.

Dataset \ Model	Ours	rSLDS	SLDS	BTMF	RKN	LSTNet
Salsa Dance	<b>6.74</b>	8.78	8.68	7.75	8.86	7.91
Bat Flight	<b>7.69</b>	9.93	10.69	8.91	17.81	16.35
Golf	10.57	10.89	13.64	<b>9.43</b>	12.60	17.87
Walking	<b>8.01</b>	21.81	22.59	31.39	23.56	14.77
Pendulum	<b>5.95</b>	25.58	29.02	21.14	8.77	8.62

Best results are highlighted in bold fonts.

sion with first-order temporal lag, denoted by **Ours w/ $\ell = \{1\}$** , and applied them on our experimental datasets. The results of test set predictions for these model variants are compared with the original model in Table 3. It is clear from the results of this table that both the switching feature (i.e., dynamical modes) and higher-order temporal modeling have consistently enhanced prediction accuracy of our model in all the experiments.

## 8 Conclusion

We proposed a deep switching dynamical model for dynamical analysis of 3D motion data. Our model was able to uncover interpretable states in the low-dimensional dynamical generative model of the data. We parameterized these low-level temporal generative models with regard to a switching deep vector autoregressive (VAR) prior to enable multimodal and higher-order dynamical

Table 3: Comparison of our proposed model with its two ablated variants in terms of prediction error (NRMSE%) on the test sets of our datasets. Both the switching feature and higher-order temporal modeling have consistently enhanced prediction accuracy of our model in all the experiments.

Dataset \ Model	Ours	Ours w/o switch	Ours w/ $\ell = \{1\}$
Salsa Dance	<b>6.74</b>	8.73	8.76
Bat Flight	<b>7.69</b>	8.34	8.72
Golf	<b>10.57</b>	11.23	11.79
Walking	<b>8.01</b>	9.85	9.88
Pendulum	<b>5.95</b>	6.91	7.54

Best results are highlighted in bold fonts.

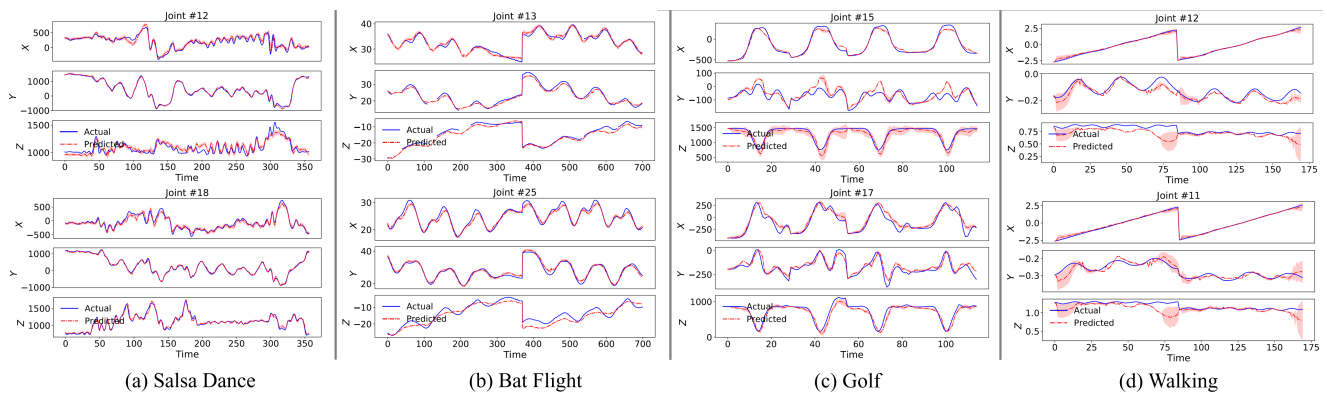


Fig. 9: Visualizations of test set predictions for two sample joints for each of the salsa dance, bat flight, golf and walking datasets. Note that our model fills in missing values in the bat flight dataset. Red-shaded regions correspond to prediction uncertainty.

cal estimation. Our segmentation, generative and predictive results on one simulated physical system and four real motion data demonstrated the superior performance of the proposed model in comparison with the state-of-the-art methods.

## References

- Ackerson G, Fu K (1970) On state estimation in switching environments. *IEEE transactions on automatic control* 15(1):10–17 [2](#)
- Bahadori MT, Yu QR, Liu Y (2014) Fast multivariate spatio-temporal analysis via low rank tensor learning. In: *Advances in neural information processing systems*, pp 3491–3499 [2](#)
- Barbič J, Safonova A, Pan JY, Faloutsos C, Hodgins JK, Pollard NS (2004) Segmenting motion capture data into distinct behaviors. In: *Proceedings of Graphics Interface 2004*, Citeseer, pp 185–194 [1](#)
- Becker P, Pandya H, Gebhardt G, Zhao C, Taylor CJ, Neumann G (2019) Recurrent kalman networks: Factorized inference in high-dimensional deep feature spaces. In: *International Conference on Machine Learning*, pp 544–552 [2](#), [5](#)
- Becker-Ehmck P, Peters J, Van Der Smagt P (2019) Switching linear dynamics for variational bayes filtering. In: *International Conference on Machine Learning*, pp 553–562 [2](#)
- Bergou AJ, Swartz SM, Vejdani H, Riskin DK, Reimnitz L, Taubin G, Breuer KS (2015) Falling with style: bats perform complex aerial rotations by adjusting wing inertia. *PLoS Biol* 13(11):e1002297 [6](#)
- Birch MC, Quinn RD, Hahm G, Phillips SM, Drennan B, Fife A, Verma H, Beer RD (2000) Design of a cricket microrobot. In: *Proceedings 2000 ICRA. Millennium Conference. IEEE International Conference on Robotics and Automation. Symposia Proceedings (Cat. No. 00CH37065)*, IEEE, vol 2, pp 1109–1114 [1](#)
- Blender Online Community (2020) Blender - a 3D modelling and rendering package. Blender Foundation, Blender Institute, Amsterdam, URL <http://www.blender.org> [6](#)
- Cai Y, Tong H, Fan W, Ji P, He Q (2015) Facets: Fast comprehensive mining of coevolving high-order time series. In: *ACM SIGKDD International Conference on Knowledge Discovery and Data Mining*, pp 79–88 [2](#)
- Chang CB, Athans M (1978) State estimation for discrete systems with switching parameters. *IEEE Transactions on Aerospace and Electronic Systems* pp 418–425 [2](#)
- Chang YY, Sun FY, Wu YH, Lin SD (2018) A memory-network based solution for multivariate time-series forecasting. *arXiv preprint arXiv:180902105* [2](#)
- Chen L, Amiri SE, Prakash BA (2018) Automatic segmentation of data sequences. In: *Proceedings of the AAAI Conference on Artificial Intelligence* [1](#), [2](#)
- Elhamifar E, Sapiro G, Sastry SS (2015) Dissimilarity-based sparse subset selection. *IEEE transactions on pattern analysis and machine intelligence* 38(11):2182–2197 [1](#)
- Farnoosh A, Azari B, Ostadabbas S (2020a) Deep switching auto-regressive factorization: Application to time series forecasting. *arXiv preprint arXiv:200905135* [2](#)
- Farnoosh A, Rezaei B, Sennesh EZ, Khan Z, Dy J, Satpute A, Hutchinson JB, van de Meent JW, Ostadabbas S (2020b) Deep markov spatio-temporal factorization. *arXiv preprint arXiv:200309779* [2](#)
- Fox E, Sudderth EB, Jordan MI, Willsky AS (2009) Nonparametric bayesian learning of switching linear dynamical systems. In: *Advances in neural information processing systems*

- tion processing systems, pp 457–464 [2](#), [5](#)
- Fraccaro M, Kamronn S, Paquet U, Winther O (2017) A disentangled recognition and nonlinear dynamics model for unsupervised learning. In: *Advances in Neural Information Processing Systems*, pp 3601–3610 [2](#)
- Ghahramani Z, Hinton GE (1996) Switching state-space models. Tech. rep., Citeseer [2](#)
- Gong C, Travers MJ, Astley HC, Li L, Mendelson JR, Goldman DI, Choset H (2016) Kinematic gait synthesis for snake robots. *The International Journal of Robotics Research* 35(1-3):100–113 [1](#)
- Gong D, Medioni G, Zhu S, Zhao X (2012) Kernelized temporal cut for online temporal segmentation and recognition. In: *European Conference on Computer Vision*, Springer, pp 229–243 [1](#)
- Gong D, Medioni G, Zhao X (2013) Structured time series analysis for human action segmentation and recognition. *IEEE transactions on pattern analysis and machine intelligence* 36(7):1414–1427 [1](#)
- Hamilton JD (1990) Analysis of time series subject to changes in regime. *Journal of econometrics* 45(1-2):39–70 [2](#)
- Hoff J, Ramezani A, Chung SJ, Hutchinson S (2016) Synergistic design of a bio-inspired micro aerial vehicle with articulated wings. In: *Robotics: science and systems* [1](#)
- Hoffman MD, Blei DM, Wang C, Paisley J (2013) Stochastic variational inference. *The Journal of Machine Learning Research* 14(1):1303–1347 [4](#)
- Jolliffe IT (1986) Principal components in regression analysis. In: *Principal component analysis*, Springer, pp 129–155 [1](#)
- Karl M, Soelch M, Bayer J, van der Smagt P (2017) Deep variational bayes filters: Unsupervised learning of state space models from raw data. *stat* 1050:3 [2](#)
- Kingma DP, Ba J (2014) Adam: A method for stochastic optimization. *arXiv preprint arXiv:1412.6980* [4](#)
- Kingma DP, Welling M (2014) Auto-encoding variational bayes. *stat* 1050:1 [4](#)
- Krishnan RG, Shalit U, Sontag D (2017) Structured inference networks for nonlinear state space models. In: *Thirty-First AAAI Conference on Artificial Intelligence* [2](#)
- Krüger B, Vögele A, Willig T, Yao A, Klein R, Weber A (2016) Efficient unsupervised temporal segmentation of motion data. *IEEE Transactions on Multimedia* 19(4):797–812 [1](#), [2](#)
- Lai G, Chang WC, Yang Y, Liu H (2018) Modeling long-and short-term temporal patterns with deep neural networks. In: *ACM SIGIR Conference on Research & Development in Information Retrieval*, pp 95–104 [2](#), [5](#)
- Li S, Jin X, Xuan Y, Zhou X, Chen W, Wang YX, Yan X (2019) Enhancing the locality and breaking the memory bottleneck of transformer on time series forecasting. In: *Advances in Neural Information Processing Systems* [2](#)
- Linderman S, Johnson M, Miller A, Adams R, Blei D, Paninski L (2017) Bayesian learning and inference in recurrent switching linear dynamical systems. In: *Artificial Intelligence and Statistics*, pp 914–922 [2](#), [3](#)
- Meshry M, Hussein ME, Torki M (2016) Linear-time online action detection from 3d skeletal data using bags of gesturelets. In: *2016 IEEE Winter Conference on Applications of Computer Vision (WACV)*, IEEE, pp 1–9 [3](#)
- Moeslund T, Hilton A, Krüger V (2006) A survey of advances in vision-based human motion capture and analysis. *Computer Vision and Image Understanding* 104(2-3 SPEC. ISS.):90–126, DOI 10.1016/j.cviu.2006.08.002 [1](#)
- Murphy KP (1998) Switching kalman filters. Citeseer [2](#)
- Nakamura T, Nagai T, Mochihashi D, Kobayashi I, Asoh H, Kaneko M (2017) Segmenting continuous motions with hidden semi-markov models and gaussian processes. *Frontiers in neurorobotics* 11:67 [3](#)
- Nassar J, Linderman S, Bugallo M, Park I (2019) Tree-structured recurrent switching linear dynamical systems for multi-scale modeling. In: *International Conference on Learning Representations (ICLR)* [2](#), [5](#)
- Papoutsakis K, Panagiotakis C, Argyros AA (2017) Temporal action co-segmentation in 3d motion capture data and videos. In: *Proceedings of the IEEE Conference on Computer Vision and Pattern Recognition*, pp 6827–6836 [1](#), [2](#)
- Paszke A, Gross S, Chintala S, Chanan G, Yang E, DeVito Z, Lin Z, Desmaison A, Antiga L, Lerer A (2017) Automatic differentiation in pytorch. *NIPS 2017 Workshop* [4](#)
- Patrona F, Chatzitofis A, Zarpalas D, Daras P (2018) Motion analysis: Action detection, recognition and evaluation based on motion capture data. *Pattern Recognition* 76:612–622 [1](#), [2](#)
- Ranganath R, Wang C, David B, Xing E (2013) An adaptive learning rate for stochastic variational inference. In: *International Conference on Machine Learning*, pp 298–306 [4](#)
- Rangapuram SS, Seeger MW, Gasthaus J, Stella L, Wang Y, Januschowski T (2018) Deep state space models for time series forecasting. In: *Advances in neural information processing systems*, pp 7785–7794 [2](#)
- Riskin DK, Willis DJ, Iriarte-Díaz J, Hedrick TL, Kostandov M, Chen J, Laidlaw DH, Breuer KS, Swartz SM (2008) Quantifying the complexity of

- bat wing kinematics. *Journal of theoretical biology* 254(3):604–615 [1](#)
- Salinas D, Flunkert V, Gasthaus J, Januschowski T (2020) Deepar: Probabilistic forecasting with autoregressive recurrent networks. *International Journal of Forecasting* 36(3):1181–1191 [2](#)
- Santello M, Flanders M, Soechting JF (1998) Postural hand synergies for tool use. *Journal of neuroscience* 18(23):10105–10115 [1](#)
- Sen R, Yu HF, Dhillon IS (2019) Think globally, act locally: A deep neural network approach to high-dimensional time series forecasting. In: *Advances in Neural Information Processing Systems*, pp 4837–4846 [2](#)
- Sun JZ, Parthasarathy D, Varshney KR (2014) Collaborative kalman filtering for dynamic matrix factorization. *IEEE Transactions on Signal Processing* 62(14):3499–3509 [2](#)
- Sun L, Chen X (2019) Bayesian temporal factorization for multidimensional time series prediction. *arXiv preprint arXiv:191006366* [5](#)
- Takeuchi K, Kashima H, Ueda N (2017) Autoregressive tensor factorization for spatio-temporal predictions. In: *2017 IEEE International Conference on Data Mining (ICDM)*, IEEE, pp 1105–1110 [2](#)
- Watter M, Springenberg J, Boedecker J, Riedmiller M (2015) Embed to control: A locally linear latent dynamics model for control from raw images. In: *Advances in neural information processing systems*, pp 2746–2754 [2](#)
- Wu Z, Liu W, Xing W (2017) A novel method for human motion capture data segmentation. In: *2017 IEEE 15th Intl Conf on Dependable, Autonomous and Secure Computing, 15th Intl Conf on Pervasive Intelligence and Computing, 3rd Intl Conf on Big Data Intelligence and Computing and Cyber Science and Technology Congress (DASC/PiCom/DataCom/CyberSciTech)*, IEEE, pp 780–787 [1, 2](#)
- Xia G, Sun H, Feng L, Zhang G, Liu Y (2017) Human motion segmentation via robust kernel sparse subspace clustering. *IEEE Transactions on Image Processing* 27(1):135–150 [1, 2](#)
- Xia G, Chen B, Sun H, Liu Q (2020) Nonconvex low-rank kernel sparse subspace learning for keyframe extraction and motion segmentation. *IEEE Transactions on Neural Networks and Learning Systems* [1, 3](#)
- Yu HF, Rao N, Dhillon IS (2016) Temporal regularized matrix factorization for high-dimensional time series prediction. In: *Advances in neural information processing systems*, pp 847–855 [2](#)
- Zhou F, De la Torre F, Hodgins JK (2012) Hierarchical aligned cluster analysis for temporal clustering of human motion. *IEEE Transactions on Pattern Analysis and Machine Intelligence* 35(3):582–596 [1](#)
- Zhou T, Fu H, Gong C, Shen J, Shao L, Porikli F (2020) Multi-mutual consistency induced transfer subspace learning for human motion segmentation. In: *Proceedings of the IEEE/CVF Conference on Computer Vision and Pattern Recognition*, pp 10277–10286 [1, 3](#)